Effects of electronic correlation, physical structure, and surface termination on the electronic structure of V_2O_3 nanowires

Amanda L. Tiano,[1] Jing-bin Li,[2] Eli Sutter,[3] Stanislaus S. Wong,[1,4,*] and M.-V. Fernández-Serra[2,†]

[1]*Department of Chemistry, State University of New York at Stony Brook, Stony Brook, New York 11794-3400, USA*

[2]*Department of Physics and Astronomy and the New York Center for Computational Science, State University of New York at Stony Brook, Stony Brook, New York 11794-3800, USA*

[3]*Center for Functional Nanomaterials, Building 735, Brookhaven National Laboratory, Upton, New York 11973, USA*

[4]*Condensed Matter Physics and Materials Science Department, Building 480, Brookhaven National Laboratory, Upton, New York 11973, USA*

(Received 7 May 2012; revised manuscript received 23 July 2012; published 26 September 2012)

We report on a density functional theory (DFT) study of the electronic structure of vanadium sesquioxide (V_2O_3) in both bulk and nanowire form. In particular, our study focuses on the role of spin polarization and electronic correlations, as computed within the local (spin) density approximation (L(S)DA) and the LDA + U formalism. As expected for a mean-field approach such as DFT, our optimized bulk V_2O_3 structure is shown to be metallic in nature, while an adequate choice of the Hubbard U parameter ($U = 4$ eV) is enough to open the band gap, making the system insulating. However, this formalism predicts a nonmagnetic insulator, as opposed to the experimentally observed antiferromagnetic structure, to be the ground state. The electronic structure of the V_2O_3 nanowire system is more complex, and it strongly depends on the surface termination of the structures. Our results show that non-spin-polarized LDA calculations of ⟨001⟩-grown nanowires are metallic in nature. However, LSDA predicts that some surface terminations are half-metals, with a large band gap opening for one of the spins. When LSDA + U was used to study the nanowire model with a closed-shell oxygen surface termination, we observe insulating behavior with no net magnetic moment, with a 104 meV band gap. This is consistent with the experimentally observed gap recently reported in the literature for similar wires. To experimentally address the surface structure of these nanowires, we perform surface specific nano-Auger electron spectroscopy on as-synthesized V_2O_3 nanowires. Our experimental results show a higher O:V peak ratio (1.93:1) than expected for pure V_2O_3, thereby suggesting higher oxygen content at the surface of the nanowires. From our results, we conclude that oxygen termination is likely the termination for our as-synthesized V_2O_3 nanowires.

DOI: 10.1103/PhysRevB.86.125135 PACS number(s): 68.47.Gh, 71.15.Mb, 61.46.Km

I. INTRODUCTION

As technology advances, the demand for miniaturization continues to be amplified, driving the need for the fabrication of device components measuring on the order of nanometers. However, within this size range, quantum mechanics begins to play a more prominent role, one that can neither be ignored nor be considered lightly. Not surprisingly, research has aimed to actively manipulate spin degrees of freedom, otherwise known as spintronics, to create the next generation of electronics.[1,2] To achieve the spin polarization required for spintronics, a great deal of interest has focused on half-metals, which are conductive in one spin orientation while insulating (or semiconducting) in the other spin orientation.[3,4] With the goal of producing viable nanoscale devices, half-metals that are low dimensional in morphology are highly desirable due to a decrease in the surface reconstructions and corresponding changes to states near the Fermi level that can lead to the destruction of the half-metallic behavior of the intended system. Numerous theoretical and experimental investigations have been conducted to determine feasible systems for spintronics applications.

One-dimensional (1D) nanostructures are among the most commonly explored nanoscale morphologies, and their inherent structural anisotropy can lead to unique and interesting optoelectronic and transport properties. In addition, many of these prospective systems contain vanadium, such as vanadium organometallics,[5–7] chalcogenides,[8] VO_x,[9] VO_2,[10] and V-doped systems.[11–13] Interestingly, vanadium-containing systems, especially the family of vanadium oxides, are notorious for possessing complex electronic structures, thereby giving rise to a range of attractive magnetic, electronic, optoelectronic, and electrochromic properties.[14,15] Recently, one of our groups synthesized vanadium sesquioxide (V_2O_3) nanorods, measuring ∼64 nm in diameter, which, upon further characterization, revealed interesting transport data. Specifically, the as-synthesized nanorods exhibited semiconducting behavior from 80 to 300 K, which had not been reported previously for their bulk counterparts. At room temperature, the nanorods display metallic-like behavior that is similar to what is expected for bulk V_2O_3. Hence, we concluded that our V_2O_3 nanorods possess a small band gap of ∼25 meV, given the observed semiconducting behavior at low temperatures and the metallic-like behavior at or above room temperature. Thus, our motivation was to investigate the nature of this electronic behavior for 1D nanoscale V_2O_3 and to draw conclusions for other analogous 1D vanadium oxides so as to explore the applicability of this family of materials for spintronics devices.

Of the family of vanadium oxides, V_2O_3 has drawn significant attention because it exhibits two metal-to-insulator transitions, which are considered classic examples of Mott transitions.[16] At room temperature, V_2O_3 is initially a paramagnetic metal (PM), but upon cooling, it changes to an antiferromagnetic insulator (AFI) at $T_N = 168$ K. Moreover, it can undergo a transition to a paramagnetic insulator phase upon doping with either chromium or aluminum or by varying

pressure.[17,18] Along with the metal-to-insulator transition from PM to AFI, V_2O_3 undergoes a structural transformation. Specifically, above T_N, it exhibits the corundum-type structure (space group $R\bar{3}c$),[19] and below T_N, V_2O_3 converts to a monoclinic structure (space group $I2/a$).[20] Arising from its magnetic, electronic, and structural transitions, the applications of V_2O_3 can be expanded to include conductive polymer composites, temperature sensors, and current regulators.[21,22]

Despite the large interest in V_2O_3, as demonstrated by the vast literature available, there is a lack of fundamental understanding in the scientific community with respect to the complexity of its electronic structure. Following the principles of crystal field theory, V_2O_3 was long considered a textbook example of the quintessential one-band Mott–Hubbard system.[23–27] However, more recent theoretical studies have challenged the validity of the conventional one-band Hubbard model in fully and accurately describing the electronic structure of V_2O_3.[28–31] Complementary experimental results[32] have supported the notion of the inadequacies of the Hubbard model for V_2O_3. Hence, attempts have been made to construct new models that can more correctly describe the electronic structure.[33–35] The most significant advances have been made with respect to the application of dynamical mean-field theory to the local density approximation (LDA)[36] treatment of V_2O_3.[37–41] Similarly, LDA + U and local (spin) density approximation (L(S)DA) + U methods[4] are commonly used as a viable approach to studying complex oxide systems containing either transition or rare-earth metals.[2,3,7,11] Inclusion of the electron Coulomb repulsion component U allows for more accurate investigations of the strong correlation effects present in these types of systems, as shown by Kresse *et al*. for the bulk V_2O_3 system.[42] Even with recent computational advances in theoretical methods, the available reports of electronic structure investigations using density functional theory (DFT) methods for bulk V_2O_3 are relatively few. To the best of our knowledge, within the family of vanadium oxides, only nanotubes of VO_2[43] and V_2O_5[44] have been investigated, and no theoretical analyses have been conducted on the precise effect of shrinking V_2O_3 to the nanoscale regime.

Herein, to address these concerns, we have performed computational investigations on both the structural and the surface termination effects on the electronic structure of 1D corundum-type V_2O_3 nanowires. The goal of our study has been twofold. First, we reanalyze the electronic structure of bulk V_2O_3 using a basis set of localized atomic orbitals, including spin polarization and electronic correlations (within the L(S)DA + U formalism) in our calculations. The first part of our work therefore serves as a validation of our method (Sec. II). In the second part of the paper, we characterize the electronic structure of V_2O_3 nanowires as a function of their surface termination to interpret our previous experimental results[45] and to investigate their potential as candidates for spintronic applications (Sec. III). In the last section of our work, we experimentally probe V_2O_3 nanowires through nano-Auger spectroscopy to investigate their surface structure (Sec. IV).

II. THEORETICAL METHODOLOGY AND CONSTRUCTS

Electronic structure calculations were conducted using DFT methods[46,47] within the LDA for both bulk and nanowire

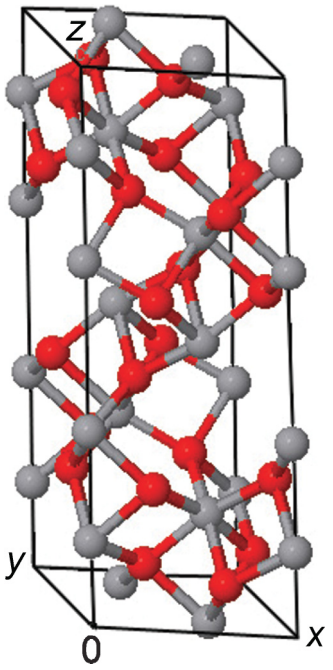

FIG. 1. (Color online) Corundum-type bulk V_2O_3 unit cell with vanadium atoms in light gray and oxygen atoms in dark gray (red online) (Ref. 50).

vanadium oxide systems using a basis set of strictly localized atomic orbitals to expand the Kohn–Sham eigenstates, as implemented in the SIESTA code.[48] We use a double-ζ polarized basis set and Troulier–Martin norm conserving pseudopotentials.[49] Structural information for the bulk V_2O_3 system was taken from crystallographic data provided by Robinson[50] and has been ascribed to the corundum-type structure (Fig. 1), which is similar to the crystallographic structure proposed by Dernier.[19] As discussed by Mattheiss,[51] there are two distinctive choices for the unit cells of the V_2O_3 structure: nonprimitive hexagonal and primitive rhombohedral. The nonprimitive hexagonal cell was used in these calculations and contains 6 formula units, consisting of 30 atoms in the unit cell. We also carried out LDA + U calculations with SIESTA. The LDA + U implementation consists of a simplified rotationally invariant LDA + U formulation[52] coupled with both ferromagnetic and antiferromagnetic ordering. Moreover, we studied the effect of the electric Coulomb repulsion parameter U in our calculations, varying it from 2.0 to 4.0 eV, given the empirical character of this particular parameter.[47] In the case of spin-polarized calculations, the system was initialized with spin polarization but with a net magnetic moment of zero, corresponding to a 50:50 population of spin-up and spin-down polarizations at every atom. However, other initial spin configurations were not investigated; therefore, the possibility that the results depend on the initial spin configuration has not been considered in this work.

Our approach contrasts with existing computational literature on V_2O_3, which tends to use the primitive rhombohedral cell. For example, in the work of Mattheiss,[51] V_2O_3 is composed of 2 formula units for 10 atoms within the unit cell. Intrinsically, there is no difference between the two unit cells.

However, the computational cost of adding more atoms renders the use of the smaller unit cell a more convenient choice. Because our unit cell contains 30 atoms, we obtain three times more electronic bands in the first Brillouin zone than do band structures calculated from the 10-atom unit cell. Brillouin zone integrations were performed using 1050 k-points for bulk V_2O_3 within the irreducible hexagonal wedge. For our V_2O_3 nanowire system, the Brillouin zone integration is performed over the range from Γ to X, where $X = \pm\pi/c$, using 150 k-points. Calculations on the bulk V_2O_3 structure have been compared with the work of Mattheiss,[51] as well as with Eyert *et al.*,[53] because the methods used in this work are similar. We also compared our LDA + U calculation results with the work of Kresse *et al.*[42]

III. THEORETICAL RESULTS AND DISCUSSION

A. Bulk V_2O_3

1. LDA

We computed the electronic structure of bulk corundum-type V_2O_3, to obtain a basis of comparison with V_2O_3 nanowires. Because our methodology was similar to the work of both Mattheiss[51] and Eyert *et al.*,[53] our goal was to produce results for bulk V_2O_3 in good agreement with both of these prior studies. However, our initial partial V 3d density of states (DOS), shown in Fig. 2 and derived from the bulk V_2O_3 structure of Robinson,[50] did not evince good separation between the two sets of bands, as compared with the previous studies of both Mattheiss[51] and Eyert *et al.*[53] The lattice parameters were systematically varied to determine the lowest energy structure using non-spin-polarized and subsequently spin-polarized calculations. The optimized lattice parameters from LDA calculations are shown in Table I, along with the crystallographic data obtained from Robinson[50] and Dernier,[19] revealing that the most significant difference is in the a value for our optimized bulk structure, specifically obtained with the LDA treatment. Differences between theory and experiment can be ascribed both to DFT approximations and to the incompleteness of our basis set.

TABLE I. V_2O_3 unit cell parameters for the optimized structures compared with those of the literature (Refs. 19 and 50).

V_2O_3 unit cell	a (Å)	c (Å)
Robinson	4.9776	13.9647
Dernier	4.952	14.003
Optimized with LDA	4.78	14.07
Optimized with LDA + U(U = 3.43 eV)	4.993	13.872

The electronic band structure results from non-spin-polarized LDA calculations on the optimized bulk V_2O_3 structure in Fig. 3(a) are shown to be in good agreement with the literature, indicating that the material is metallic in nature, which is an expected result from standard DFT calculations. Moreover, we observe three major sets of bands near the Fermi level (E_F = 0 eV): from −9.1 to −3.8 eV (data not shown), from −1.26 to 1.4 eV, and from 2.2 to 4.7 eV. The energy ranges for these bands are also consistent with previous electronic structure calculations on V_2O_3. The origin of the first set of bands, which is not shown in Fig. 3(a), can be attributed to the O 2p states. The upper two sets of bands are derived from the V 3d states, specifically the t_{2g} and e_g^{σ} states, as confirmed by subsequent partial DOS calculations (data not shown). In addition, calculations including spin polarization were conducted on the optimized bulk structure. The results, shown in Fig. 3(b), are inherently similar to their

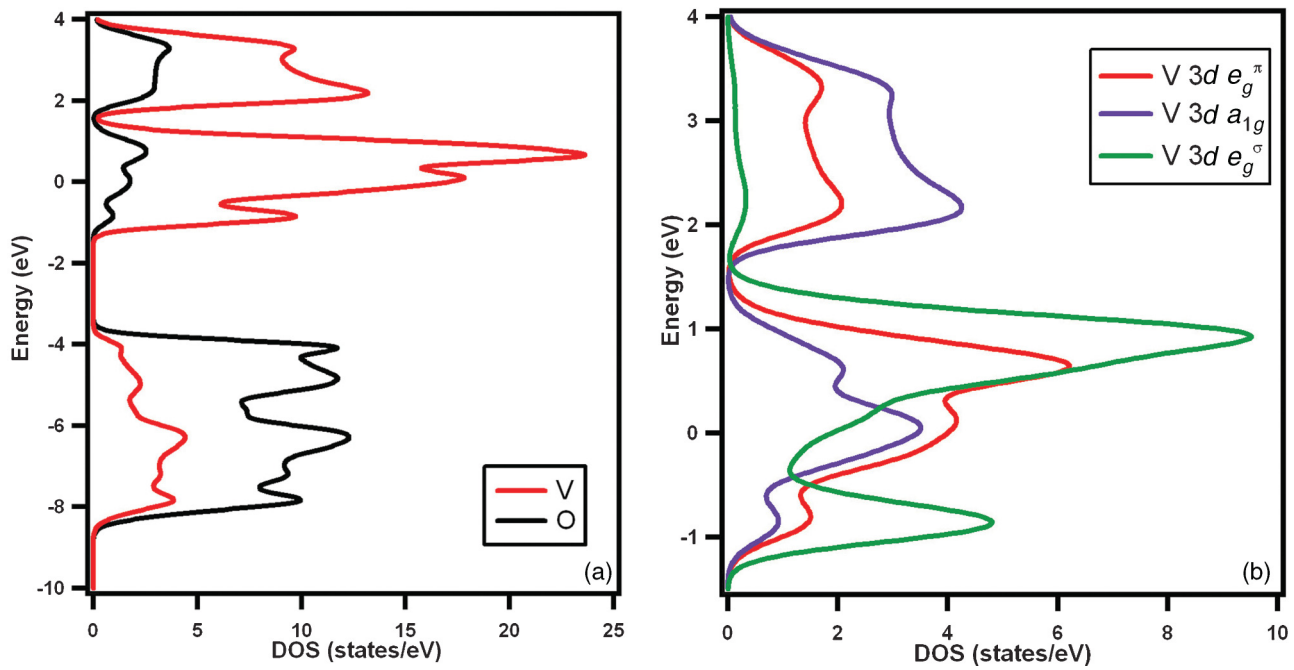

FIG. 2. (Color online) Projected electronic DOS for (a) hexagonal V_2O_3 and (b) partial V 3d DOS using crystallographic data provided by Robinson (Ref. 50).

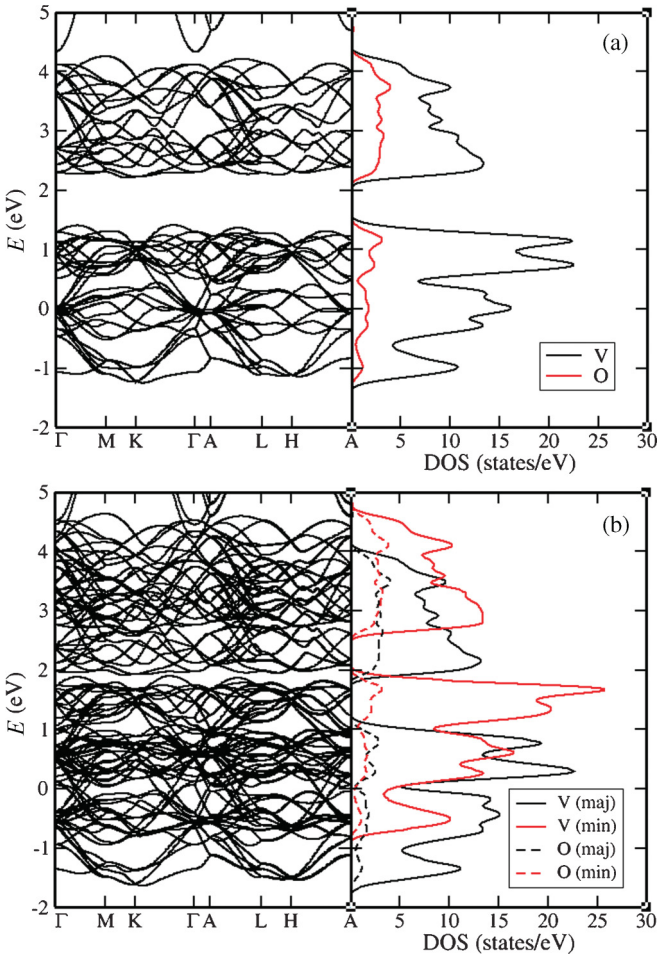

FIG. 3. (Color online) Electronic band structure and corresponding DOS for the optimized bulk V_2O_3 structure both (a) without and (b) with spin polarization.

nonspin counterparts; the electronic bands and DOS maintain the same structure with more bands present.

2. *LDA + U*

LDA + U calculations for bulk V_2O_3 show much better agreement with the experimental values for lattice parameters (Table I). This fact can be attributed to the inclusion of onsite Coulomb repulsion, which increases the distance between atoms. We also observed that as U increases, cell parameter a increases while parameter c decreases, as shown in Table II. The reason for this observation is that the U correction affects V $3d$ π and σ bonds in different ways. As shown in Fig. 1, neighboring vanadium atoms in the ab plane form a $3d$ π bond. As U increases, the strength of π bonds (already weaker than σ bonds) is reduced. Hence, the vanadium atoms move away from each other. Along the z axis, strong σ bonding tends to reduce the distance between nearby ab layers as the V $3d_{z^2}$ component becomes more localized. Moreover, as U increases, we observed separation between the t_{2g} and e_g^σ states, as shown in the V $3d$ projected DOS [Fig. 4(a)–4(c)]. We conducted additional calculations with antiferromagnetic ordering, wherein neighboring layers perpendicular to the z axis are set to possess opposite spins. The projected DOS graph of bulk V_2O_3 with antiferromagnetic ordering [Fig. 4(d)] shows a clear band gap, indicating that the antiferromagnetic bulk V_2O_3 structure is an insulator.

TABLE II. V_2O_3 unit cell parameters for the LDA + U optimized structure with U = 2.0, 3.0, and 4.0 eV.

U (eV)	a (Å)	c (Å)
2.0	4.942	13.939
3.0	4.971	13.920
4.0	5.021	13.803

3. *LSDA + U*

Band structure results from the spin-polarized LSDA + U calculations, conducted using spin polarization with the net unit cell moment set to zero, are shown in Fig. 5(a)–5(c). These results demonstrate that bulk V_2O_3 is a metal for U values ranging from 2.0 to 3.0 eV. However, it becomes a semiconducting oxide as we increase the Coulomb potential to 4.0 eV. These data indicate that the large onsite Coulomb repulsion correction substantially reduces hybridization between the V $3d$ e_g^σ and the O $2p$ states. We believe that this is why Kresse's results[42] show bulk V_2O_3 to be a semiconductor. Based on these results, bulk V_2O_3 can be described as a metallic structure with no net magnetic moment in V and a total energy slightly lower (262 meV/unit cell) than that calculated with antiferromagnetic ordering.

B. V_2O_3 nanowire

1. *Nanowire construction*

Because our data for the bulk V_2O_3 are consistent with the literature, thereby validating the methods we have employed, we constructed our V_2O_3 nanowires using these optimized bulk lattice parameters. Specifically, our nanowires were constructed from the optimized bulk corundum-type V_2O_3 unit cells. The axis of the nanowires is chosen to be along the z axis, namely, in the [001] direction, and cut in the x and y directions from a central vanadium atom at a chosen radius determined by our desired surface termination. Consistent with the literature on thin films of V_2O_3, various surface terminations are possible: (1) a half-metal V layer, which is stable under reducing conditions; (2) a full metal V_2 layer, which is stable under very reducing conditions; (3) an O_3 layer termination, which is stable in oxygen-rich environments; and (4) vanadyl (V = O) groups, which have been theoretically shown as the most stable termination over an entire range of oxygen potentials.[54,55] We have chosen to investigate the latter three surface terminations for our V_2O_3 nanowires shown in Fig. 6, and these are referred to as **NW-V** (148 atoms), **NW-O1** (184 atoms), and **NW-O2** (238 atoms), respectively. Further differences in these three nanowire structures are discussed separately in the sections that follow, including variables such as composition, radii, bonding, and the chemical state of the surface atoms or ions.

(a) *NW-V*. **NW-V** [Fig. 6(a)] was constructed to mimic a full metal layer of vanadium as the nanowire surface termination. First, all three wires have 76 vanadium atoms but vary in

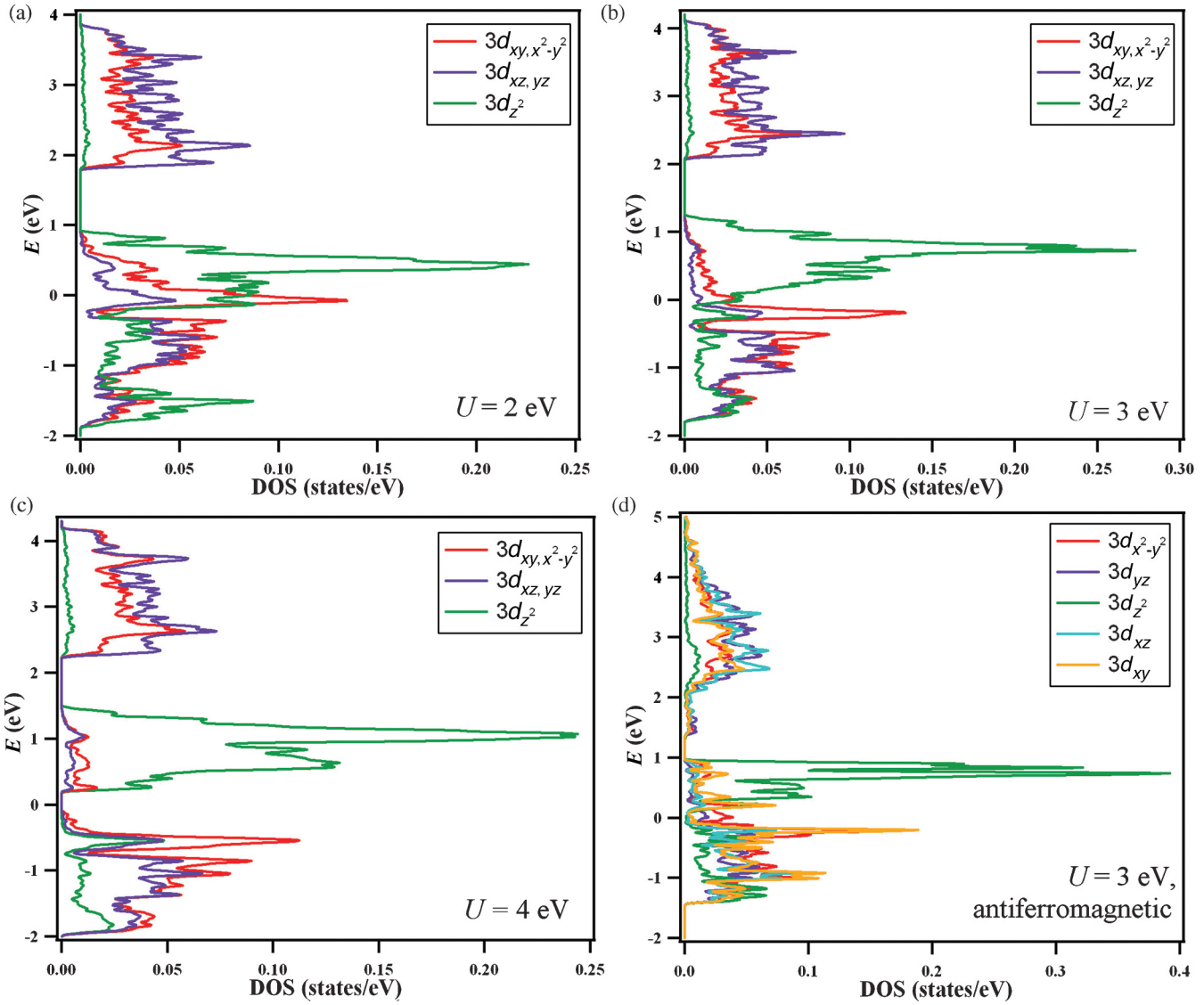

FIG. 4. (Color online) Projected DOS for the optimized bulk V_2O_3 structure with spin-polarized calculations, where the net unit cell moment is set to zero for (a) $U = 2$ eV, (b) $U = 3$ eV, (c) $U = 4$ eV, and (d) antiferromagnetic ordering for $U = 3$ eV.

composition due to the number of oxygen atoms present. As such, the vanadium-terminated surface leaves **NW-V** with 72 oxygen atoms, the least of the three nanowires analyzed. The radius of the as-constructed nanowire was calculated at 5.75 Å. At the surface, the vanadium atoms have varied coordination spheres. They alternate around the circumference of the wire with coordination to either two or three oxygen atoms, which, under the periodic boundary conditions, act as μ^4 bridging ligands between the metal atoms. As V^{3+} ions, those coordinated to three oxygen atoms are closed shell and stable. The remaining vanadium ions coordinated to two oxygen atoms are open shell, but metal-to-metal bonding with the nearest or two nearest vanadium ions yields a closed-shell configuration and hence a chemically stable nanowire surface.

(b) *NW-O1*. The second nanowire, **NW-O1** [Fig. 6(b)], was constructed with the intention of modeling the O_3 surface termination and has 108 oxygen atoms. The radius of **NW-O1** is slightly larger than that of **NW-V** at 6.09 Å. However, the surface is not composed of O_3 molecules but rather contains oxygen atoms that are bonded to either two or three vanadium atoms in bent or trigonal pyramidal geometries, respectively. Again, as with **NW-V**, all oxygen atoms have sufficient bonding to satisfy the O^{2-} ion, making all oxygen atoms closed shell. Thus, the surface herein is a chemically stable termination.

(c) *NW-O2*. **NW-O2** [Fig. 6(a)] was constructed as a model for the vanadyl (V = O) group-terminated surface and contains 162 oxygen atoms, the most of the three nanowire structures analyzed. The O:V ratio of **NW-O2** structure is the closest to our experiment data (1.93:1) among the three structures studied. Because **NW-O2** has the highest number of atoms, it is also significantly larger in the radial direction, with a radius of 6.68 Å. Because the surface was designed with the intention of modeling the V = O groups, the surface is composed of oxygen atoms bonded to vanadium atoms. The bond lengths for these groups measure either 1.97 or 2.06 Å. The bond length of vanadyl groups has been studied, and the threshold for the double bond is accepted at lengths

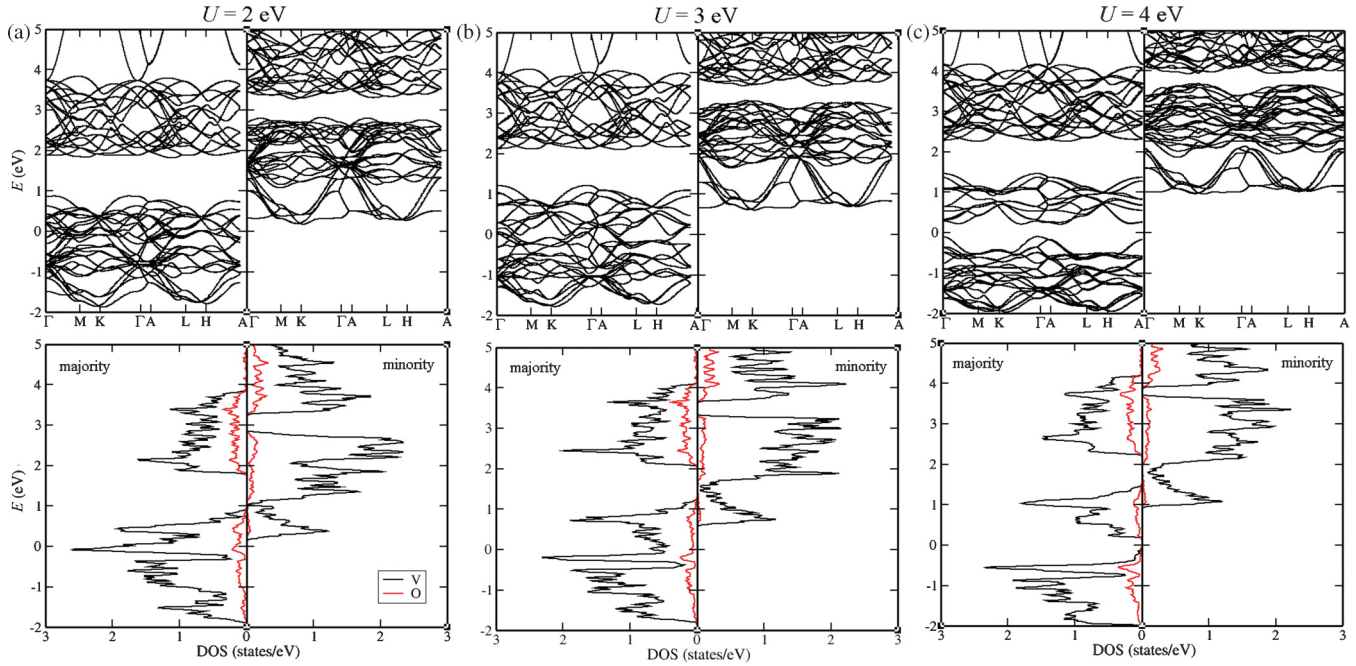

FIG. 5. (Color online) Electronic band structure and the corresponding DOS for the optimized bulk V_2O_3 structure using (a) $U = 2.0$ eV, (b) $U = 3.0$ eV, and (c) $U = 4.0$ eV. All systems are calculated with the net unit cell magnetic moment set to zero. Densities for vanadium and oxygen are shown as black and dark gray (red) lines, respectively.

shorter than 1.74 Å.[56] Because the bond lengths at the surface are above this maximum value, the groups at the surface of our nanowire consist of singly bonded oxygen atoms, leaving the exposed surface consisting of open-shell oxygen atoms. We can reasonably assume that the **NW-O2** surface is unstable, as compared with the closed-shell V = O groups, which we expected to model as the surface termination.

To investigate our V_2O_3 nanowires, we independently studied the effect of (1) c, the unit cell length for the **NW-O2** nanowire structure; (2) surface termination; and (3) structure relaxation on the resulting electronic structures. We only optimized the value of the c lattice parameter for **NW-O2** due to large surface stresses that prevented structural relaxation of the nanowires. **NW-V** and **NW-O1** were more structurally stable; hence, relaxation could be accomplished by using the optimized value ($c = 14.07$ Å) we had derived for the bulk. All wire calculations are performed for tetragonal unit cells. Wires are periodic along the c axis, and periodic images are separated by more than 40 Å of vacuum in the directions perpendicular to the wire axis. This unit cell choice hence ensures the effective unidimensionality of the calculated wires. Herein, we have discussed the effect of structural relaxations upon the V_2O_3 nanowires. Specifics regarding the effects of the unit cell length and surface termination on the electronic structure can be found in the Supplemental Material.[59]

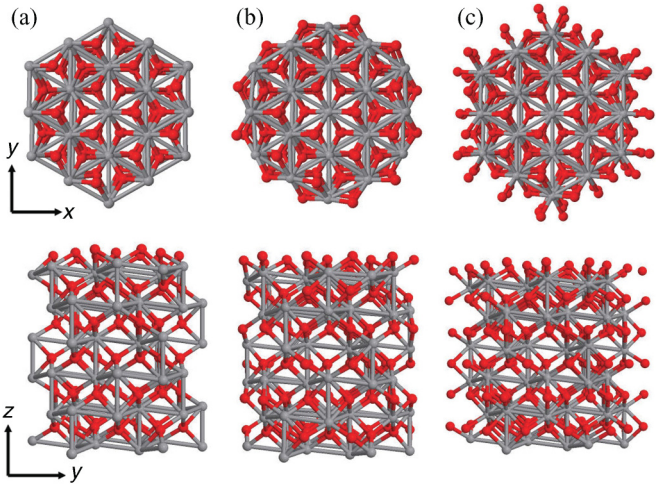

FIG. 6. (Color online) Nanowire surfaces terminated with (a) a single V, (b) an O_3 layer, and (c) a V = O layer, respectively. Vanadium atoms are shown in light gray, and oxygen atoms are highlighted in dark gray (red online).

2. *Effect of structural relaxations on electronic structure*

Each of the as-constructed nanowires was relaxed to determine the minimum energy geometry and thereby decrease the system stresses. Specifically, the system was relaxed until the overall forces were less than 0.1 eV/Å. Following the relaxation process, the band structure of the system was calculated for comparison. Only relaxations for **NW-Va** and **NW-O1a** were successful when $c = 14.07$ Å; a comparable relaxation for the **NW-O2a** structure was accomplished with an optimized unit cell length of $c = 12.90$ Å. This difference in the c lattice parameter may be a consequence of the presence of initial unstable open-shell oxygen atoms inducing large reconstructions at the surface. Moreover, these relaxations were only achieved with the exclusion of spin-polarization considerations from the calculations. The final structures for all three nanowires are shown in Fig. 7, along with the

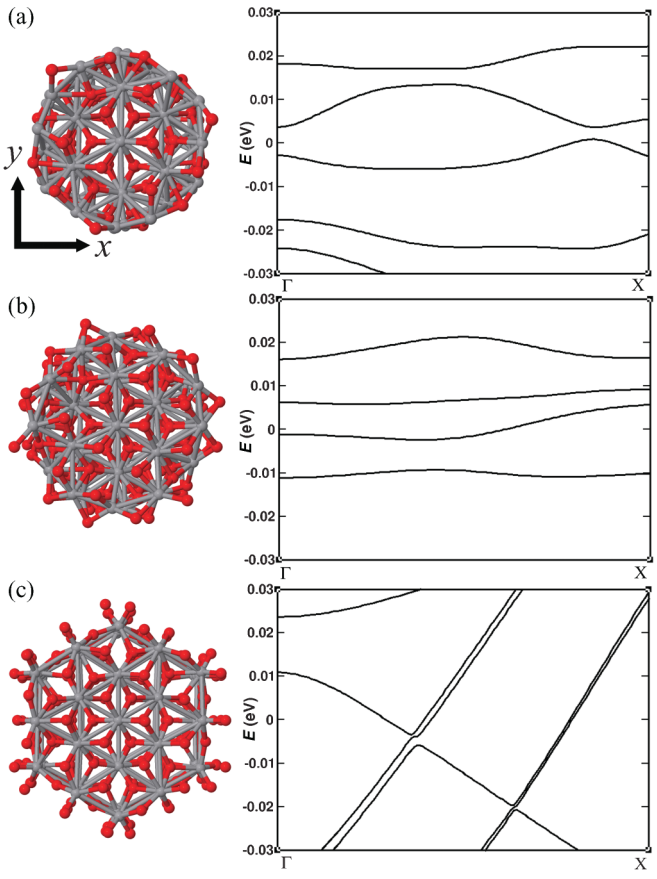

FIG. 7. (Color online) Nanowire structures, along with the corresponding electronic structure for (a) **NW-V**, (b) **NW-O1**, and (c) **NW-O2** after relaxation without spin polarization.

corresponding electronic structures for each. In addition, the data for several parameters for the initial and relaxed structures are shown in Table III.

(a) *NW-V*. The resulting structure for the vanadium surface-terminated nanowire in Fig. 7(a) is different from the initial construction, shown in Fig. 6(a). The surface atoms have compressed the nanowire in the xy direction, resulting in a narrower wire with a radius of 5.23 Å, compared with the initial radius of 5.75 Å, and translating to an ∼10% decrease in size. In addition, the oxygen atoms closest to the surface in the initial as-constructed structure are now physically closer together and even protrude outward from the surface of the nanowire. This situation may suggest that the structure would be more stable with the oxygen atoms residing at the surface. In addition to lowering energy, the stresses within the system are decreased upon relaxation. Closer analysis shows that the presence of vanadium atoms at the surface leads to a high total surface charge. While the vanadium atoms at the surface maintain a chemically stable closed-shell configuration, these data are consistent with the idea of this type of surface termination as being quite structurally unstable, in agreement with the idea of the reconstruction of the nanowire system during relaxation, leading to a net movement of oxygen atoms to the surface.

The resulting band structure for **NW-V** [Fig. 7(a)] also shows a dramatically different structure, as compared with that of the previous set of calculations (Figs. S1 and S2 in the Supplemental Material[59]). The nanowire is clearly semiconducting in nature, with an indirect band gap around the Fermi level of ∼9 meV and with few bands present around the Fermi level. Moreover, what is apparent in Fig. 7(a) is the lack of symmetry present in the final relaxed structure. It is clear that one side of the nanowire is more compressed than the other in the x and y directions. This lack of symmetry causes the opening of some small gaps, which appear as a result of the formation of discrete bands in the electronic structure plots. Moreover, the electronic structure of **NW-V** is distinctive, as compared with the optimized bulk V_2O_3 structure, because there are many differences present in the electronic structures in Figs. 7(a) and 3(b), respectively. Although there is a dominant contribution from vanadium around the Fermi level, which is similar to bulk V_2O_3, we believe that the semiconducting behavior observed in the electronic structure data for **NW-V** is a consequence of the rearrangement of the oxygen atoms toward the surface and their interaction with the V atoms. Thus, as we see with **NW-O1**, the surface plays a crucial role in determining the ensuing electronic behavior of V_2O_3 nanowires.

(b) *NW-O1*. As with **NW-V**, the core of the nanowire structure in **NW-O1** is compressed toward the center following relaxation. This is confirmed by the decrease in radius from 6.09 to 5.63 Å after relaxation, which corresponds to a 7.6% radial decrease. However, this structure is dramatically

TABLE III. Various LSDA calculated parameters for **NW-V**, **NW-O1**, and **NW-O2** (LSDA and LSDA + U) at c = 14.07 Å, for the as-constructed surface (i) and after relaxation (f).

Parameter	**NW-V**	**NW-O1**	**NW-O2** (LSDA)	**NW-O2** (LSDA + U)
r_i (Å)	5.75	6.09	6.68	6.68
r_f (Å)	5.23	5.63	5.53	6.52
Average surface charge	12.55 per V atom	6.56 per O atom	6.36 per O atom	6.42 per O atom
Magnetization ($Q_{up} - Q_{down}$)	17.1256	151.53	11.8495	56.00
		Average bond lengths (Å)		
V-V	2.63 ± 0.33	2.69 ± 0.28	2.88 ± 0.24	2.80 ± 0.21
V-O (bulk)	2.01 ± 0.05	1.97 ± 0.06	1.99 ± 0.24	1.89 ± 0.13
V-O (surface)	1.96 ± 0.11	1.90 ± 0.09	1.69 ± 0.11	2.08 ± 0.21
Band gap (eV)	0.034 (minority)	0.010 (minority)	N/A	0.066 (majority), 2.047 (minority)

different in that the oxygen atoms on the surface appear to be expanding out from the center, forming a more pyramidal or bent geometry and thereby causing them to protrude farther from the core of the nanowire. In addition, Table III shows that the surface charges for **NW-O1** are significantly lower, as compared with **NW-V**, an observation emphasizing the stability of the V_2O_3 nanowire composed of O-terminated surfaces.

In the analysis of the electronic structure of **NW-O1**, it is clear that this wire also results in a different electronic structure from that of as-constructed nanowires and rather closely resembles the relaxed **NW-V** electronic structure. Figure 7(b) shows that the relaxed **NW-O1** structure also yields a small indirect semiconducting gap present around the Fermi level of ∼3.2 meV. Moreover, the bands present around the Fermi level appear to be discrete from one another, likely an outcome of symmetry breaking to a similar extent that was observed for **NW-V**, as evidenced by the relatively larger gaps in the electronic structure for **NW-O1**. Because the oxygen atoms contribute little to the electronic structure in this range, the observed semiconducting gap can clearly be ascribed to a lack of electronic states from the vanadium atoms. One question still to be addressed is whether the origin of the band gap is symmetry induced or if it is a pure intrinsic effect, associated with the surface termination and reconstruction of this nanowire. We believe that the oxygen surface termination is a necessary condition for achieving semiconducting behavior in the wire. The reason for this assertion is that the bands around the Fermi level of this termination are less dispersive than V bands. While disorder might play an effect, this is a surface disorder phenomenon that is not core induced and hence will be always present in these structures.

(c) *NW-O2*. Consistent with the other two nanowire structures, **NW-O2** is compressed in the xy direction upon relaxation. However, the change is not as drastic as with the former two, as evinced by the slight radial decrease (e.g., 2.2%) from 6.68 to 6.53 Å. More importantly, the length of the surface V-O bonds has decreased drastically to 1.59 Å, which is well within the accepted lengths for V = O groups. Thus, we have shown that relaxing the constructed nanowires has produced a more chemically stable surface termination, because these bonds now model a closed-shell system. Moreover, the surface charges on the oxygen atoms are similar to those of **NW-O1**.

Analysis of the electronic structure in Fig. 7(c) for the relaxed **NW-O2** structure reveals a drastically different set of bands, as compared with those associated with both relaxed structures for **NW-V** and **NW-O1**, as well as with the as-constructed **NW-O2** nanowire shown in Fig. 6(c). Unlike **NW-V** and **NW-O1**, there is no gap around the Fermi level, which clearly evinces a metallic band structure that is highly reminiscent of the electronic structure calculated for the optimized bulk V_2O_3 structure in Fig. 3(b). Although **NW-O2** is shown to be metallic, the bands around the Fermi level are still dominated by the vanadium atoms. These data reaffirm the importance of the oxygen surface construction about the outer vanadium atoms; in effect, the presence of V = O groups appears to make **NW-O2** metallic in nature.

Based on these results, we can easily conclude that the **NW-O2** surface construction is bulk-like in behavior and is not consistent with our previous experimental data on as-synthesized V_2O_3 nanowires. It is clear that the number and positioning of the oxygen atoms on the surface play critical roles in determining the electronic behavior of the

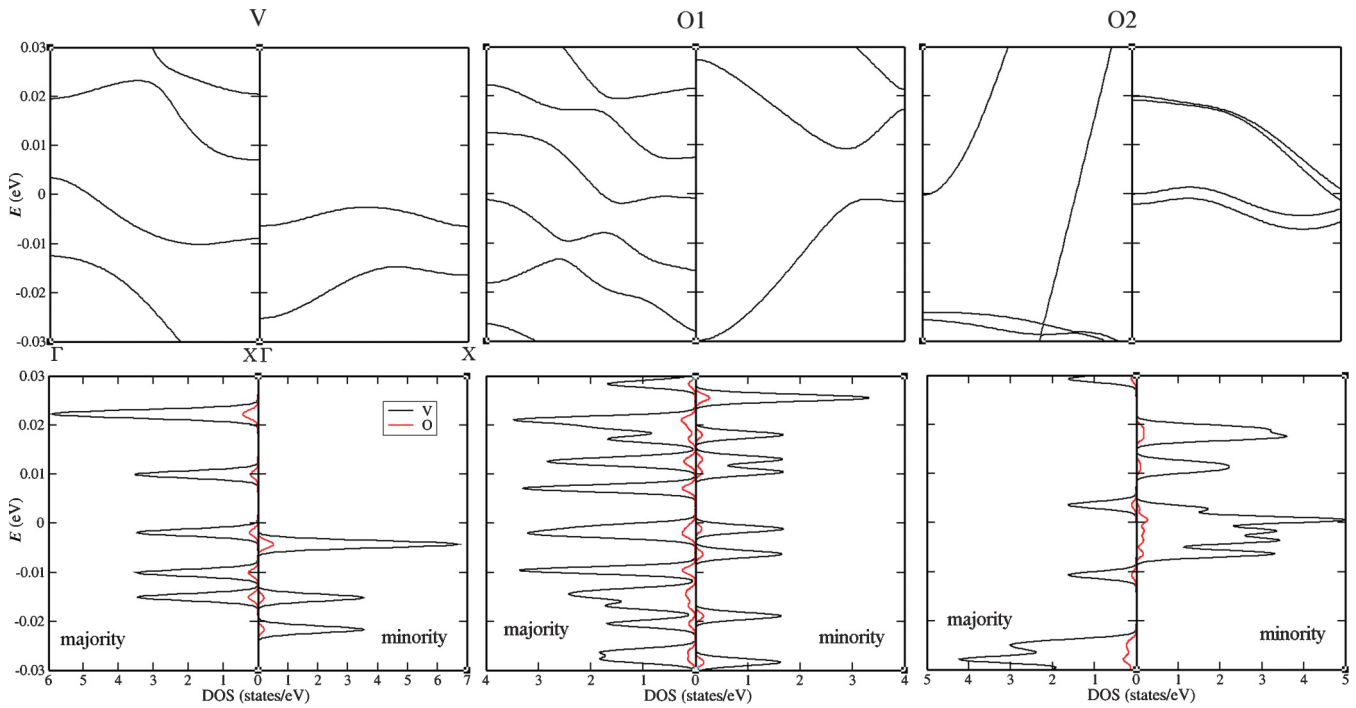

FIG. 8. (Color online) Electronic structure (top) and DOS (bottom) for **NW-V**, **NW-O1**, and **NW-O2**, calculated using spin polarization and plotted with respect to both majority and minority spin components. Densities for vanadium and oxygen are shown as black and dark gray (red) lines, respectively.

V_2O_3 nanowires. The tendency of **NW-V** to move oxygen atoms toward the surface upon relaxation is further evidence of this trend. The electronic structures of both **NW-V** and **NW-O1** most closely resemble our experimental data, because both model nanowires possess an intrinsic semiconducting gap around the Fermi level. It may be more likely that the structure and surface of **NW-V** are most consistent with our experimental data and reaction conditions, namely, the controlled presence of a reducing atmosphere, which would logically result in the formation of a proportionally higher number of vanadium atoms at the surface of our as-synthesized V_2O_3 nanowires. However, because both nanowire structures have undergone surface reconstructions during relaxation processes, resulting in both oxygen-terminated surfaces, we can conclude that both **NW-V** and **NW-O1** are viable surface compositions of our as-synthesized nanowires.

3. LSDA results with relaxed NW-V, NW-O1, and NW-O2 nanowires

To investigate the applicability of the V_2O_3 nanowires for spintronics applications, we repeated calculations on our optimized nanowire structures with the inclusion of spin polarization within the LDA algorithm. The corresponding results are shown in Fig. 8. It is clear that all three nanowires are spin polarized, as evidenced by the magnetization values shown in Table III. Compared with their non-spin-polarized counterparts (Fig. 7), the electronic results are drastically different. In the cases of **NW-V** and **NW-O1**, the nanowires are shown to be half-metallic in nature. Specifically, the majority spin component is metallic, whereas the minority spin analogue is semiconducting with gaps present near the Fermi level, as evidenced by the DOS results. The **NW-O2** system behaves differently, as compared with the other two nanowire systems. In this case, the majority spin component is metallic in nature, but there is no corresponding semiconducting gap present in the minority spin element. However, a more detailed study of the bands close to the Fermi level from the minority spin scenario shows the potential to have created a gap so as to induce spin polarization for this nanowire structure. Not surprisingly, all DOS results have shown that the vanadium atoms heavily dominate the electronic states about the Fermi level, which is an observation consistent with our non-spin-polarized calculations on V_2O_3 nanowires.

4. LSDA + U results with relaxed NW-O2 nanowire

Though the LSDA calculation results of our **NW-O2** nanowire suggest that it is a metal, our experiments predict high O concentration at the nanowire surface. Therefore, we performed LSDA + U calculations on **NW-O2** without magnetic ordering. We chose U to be 3.43 eV, the same value used by Kresse *et al.*[42] Our calculation results show c = 13.53 Å for the optimized structure, which is 0.63 Å larger than the optimized parameter, c = 12.9 Å, derived from LSDA calculations. Within the LSDA formalism, the surface O atom [Fig. 6(c)] forms very strong bonds with neighboring V atoms, with bond lengths of 1.69 Å, because these are consistent with vanadyl (V = O) bond lengths.[56] These V-O bonds pull nearby *ab* vanadium planes closer to each other, which explains why the NW-O2 results possess a smaller c value than the NW-V and NW-O1 results.

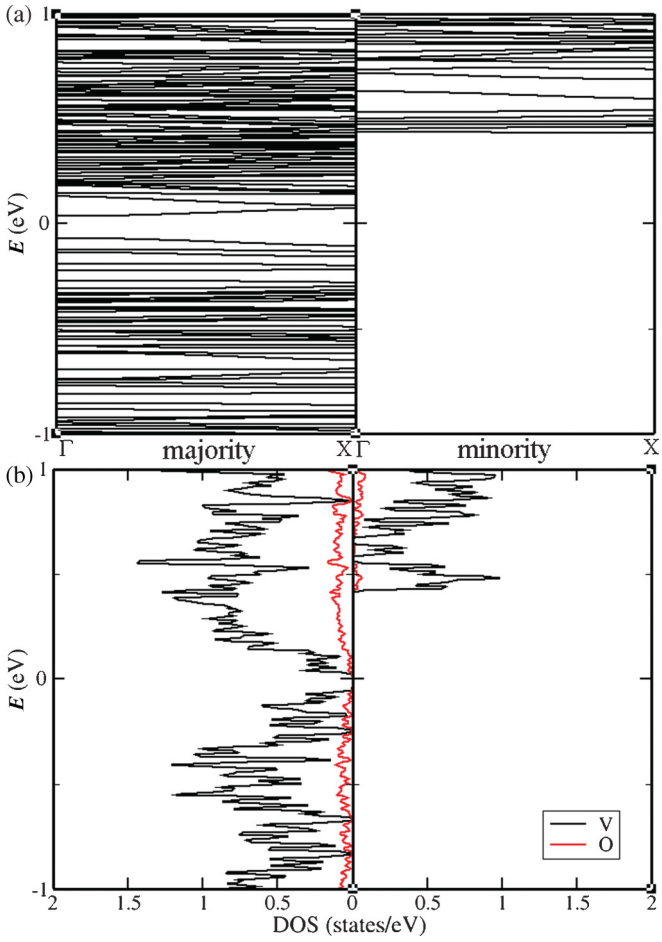

FIG. 9. (Color online) (a) Electronic band structure and (b) corresponding DOS for the V_2O_3 nanowire with the net unit cell magnetic moment set to zero. Densities for vanadium and oxygen are shown as black and dark gray (red) lines, respectively.

As discussed in the bulk LSDA + U section, including an onsite Coulomb repulsion correction substantially reduces hybridization between the V 3d e_g^σ and the O 2p states, thereby increasing the surface V-O bond length to 2.06 Å, which in turn increases the unit cell length in the z direction. The band structures, as shown in Fig. 9(a) and 9(b), show that small band gaps are present. Specifically, the majority spin has a ∼104 meV gap, while the minority spin has a 2.047 eV gap (Table III). These results agree well with our experimental observation that the nanowire is semiconducting in nature.

IV. SURFACE EXPERIMENTAL VERIFICATION OF THEORETICAL RESULTS

A. Experimental methods

V_2O_3 nanowires were synthesized following a protocol developed by one of our groups.[45] First, an aqueous solution of V_2O_5 is mixed with KOH and hydrazine, followed by a pH adjustment to ∼3 by dropwise addition of HCl. The reaction mixture is hydrothermally treated at 150 °C for 48 h, producing VO_2 nanorods. These as-synthesized VO_2 nanorods are then

heated at a ramp rate of 30 °C/min to 700 °C and subsequently held for 1 h in a reducing atmosphere (Ar/H_2) to form V_2O_3 nanowires.

Powder samples for x-ray diffraction (XRD) analysis were prepared by forming a slurry via sonication in absolute ethanol (Acros Organics, 99.5 + %) that was deposited onto glass slides and dried. The analysis was conducted using a Scintag diffractometer operating in the Bragg configuration using Cu Kα radiation ($\lambda = 1.54$ Å) and scanned over a range of 20° to 80° in 2θ, with a 1° step size. Sample preparation for scanning electron microscopy (SEM) and nano-Auger electron spectroscopy characterization was conducted by dispersion of the as-prepared product in ethanol, followed by evaporation onto a silicon wafer. The morphology and sizes of the final products were investigated using a Hitachi S-4800 field emission (FE) SEM. Nano-Auger electron spectroscopy was performed using an Omicron Nanotechnology system equipped with an ultrahigh-vacuum (UHV) FE-SEM and Auger electron analyzer, with excitation of the Auger electrons achieved using a focused SEM electron beam (10 keV, 100 pA).

B. Results

The resulting XRD pattern for the as-prepared sample could be indexed to the corundum-type V_2O_3 (Joint Committee on Powder Diffraction Standards No. 85-1411) with the space group $R\bar{3}c$ (Fig. S3 in the Supplemental Material[59]). A corresponding SEM analysis revealed that as-synthesized V_2O_3 possessed a nanowire morphology, as expected. Moreover, the thin V_2O_3 nanowires measured 27 ± 4 nm in diameter and up to several microns in length (Fig. S4 in the Supplemental Material[59]).

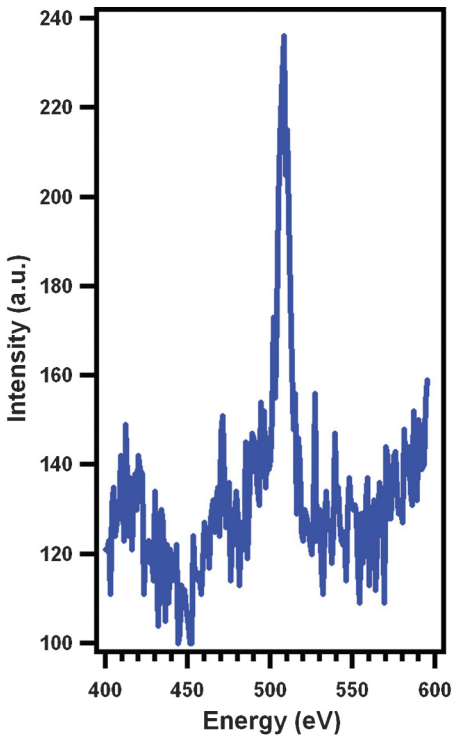

FIG. 10. (Color online) UHV nano-Auger electron spectrum obtained from the surface of a V_2O_3 nanowire, showing the presence of both vanadium (437 and 473 eV) and oxygen (514 eV) peaks.

To compare theoretical results on the surface termination effects with actual experimental data, we probed the nanowire surface with nano-Auger electron spectroscopy to determine elemental composition. Nano-Auger detected the presence of both vanadium (437 and 473 eV) and oxygen (514 eV) on the external nanowire surface (Fig. 10), with minor shifts in the peak locations observed. However, this is consistent with the difference in the oxidation state of the vanadium in V_2O_3 with respect to pure vanadium.[57] Because the sample was stored in a glove box and subsequently moved to the UHV SEM system for analysis, the likelihood of other oxygen-containing adsorbates is significantly decreased, thereby rendering the ratio of the O:V (514:437 eV) peaks more reliable for stoichiometric measurements. In our spectrum, the intensities of these two peaks were determined to be 1.93:1, which is slightly higher than the expected value for V_2O_3.[58] Because XRD analysis confirmed the presence of pure V_2O_3 with no impurities, the O:V ratio suggests that there is higher oxygen content at the surfaces of the nanowires. This experimental observation is in agreement with our theoretical results. Hence, it is highly likely that the as-synthesized V_2O_3 nanowires are oxygen-terminated.

V. CONCLUSIONS

We have presented here a detailed study[59] of the electronic and atomic structure of three surface-terminated V_2O_3 nanowires and performed a detailed comparison with the bulk V_2O_3 system. Our study has paid detailed attention to the role of electronic correlations, as described by the LDA + U approximation. Both spin-polarized and non-spin-polarized calculations have been performed. We have shown that the electronic structure nature of the V_2O_3 nanowire system is more complex than its bulk counterpart and strongly depends on the surface termination of the structures.

Specifically, our results show that non-spin-polarized LDA calculations of ⟨001⟩-grown nanowires are metallic in nature. However, LSDA predicts some surface terminations to be half-metals, with a large band gap opening for one of the spins. When LSDA + U was used to study the nanowire model with a closed-shell oxygen surface termination, we observed insulating behavior with no net magnetic moment in V, coupled with a 104 meV band gap. This result is consistent with the experimentally observed gap recently reported in the literature for similar wires by one of our groups.[45] In addition, analysis of as-synthesized V_2O_3 nanowires via nano-Auger electron spectroscopy demonstrated a larger O (514 eV)-to-V (437 eV) peak ratio than expected for bulk, suggesting that the oxygen content is higher at the surfaces of the nanowires. We can therefore reasonably conclude that the as-synthesized V_2O_3 nanowires are oxygen-terminated and that this termination is the most stable among all other credible possibilities.

ACKNOWLEDGMENTS

M.V.F.S. was funded by US Department of Energy (DOE) Award No. DE-FG02-09ER16052. J.L. acknowledges support

from Multidisciplinary University Research Initiative Award No. FA9550-12-1-0038. This research utilized resources at the New York Center for Computational Sciences at Stony Brook University/Brookhaven National Laboratory, which is supported by the DOE under Contract No. DE-AC02-98CH10886 and by the State of New York. Research (including support for A.L.T. and S.S.W.) was supported by the DOE's Basic Energy Sciences, Materials Sciences and Engineering Division. Auger experiments in this manuscript were performed at the Center for Functional Nanomaterials located at Brookhaven National Laboratory, which is supported by the DOE under Contract No. DE-AC02-98CH10886.

*stanislaus.wong@stonybrook.edu
†maria.fernandez-serra@stonybrook.edu

[1]S. A. Wolf, D. D. Awschalom, R. A. Buhrman, J. M. Daughton, S. von Molnar, M. L. Roukes, A. Y. Chtchelkanova, and D. M. Treger, Science **294**, 1488 (2001).
[2]D. D. Cuong, B. Lee, K. M. Choi, H.-S. Ahn, S. Han, and J. Lee, Phys. Rev. Lett. **98**, 115503 (2007).
[3]O. Bengone, M. Alouani, P. E. Blöchl, and J. Hugel, Phys. Rev. B **62**, 16392 (2000).
[4]V. Anisimov, F. Aryasetiawan, and A. I. Lichtenstein, J. Phys. Condens. Matter **9**, 767 (1997).
[5]S. S. Mallajosyula, P. Parida, and S. K. Pati, J. Mater. Chem. **19**, 1761 (2009).
[6]V. V. Maslyuk, A. Bagrets, V. Meded, A. Arnold, F. Evers, M. Brandbyge, T. Bredow, and I. Mertig, Phys. Rev. Lett. **97**, 097201 (2006).
[7]F. Zhou, C. A. Marianetti, M. Cococcioni, D. Morgan, and G. Ceder, Phys. Rev. B **69**, 201101 (2004).
[8]X. Wen-Hui and L. Bang-Gui, J. Phys. Condens. Matter **15**, 5085 (2003).
[9]L. Krusin-Elbaum, D. M. Newns, H. Zeng, V. Derycke, J. Z. Sun, and R. Sandstrom, Nature **431**, 672 (2004).
[10]K. G. West, J. Lu, L. He, D. Kirkwood, W. Chen, T. P. Adl, M. S. Osofsky, S. B. Qadri, R. Hull, and S. A. Wolf, J. Supercond. Novel Magn. **21**, 87 (2008).
[11]C. Loschen, J. Carrasco, K. M. Neyman, and F. Illas, Phys. Rev. B **75**, 035115 (2007).
[12]C.-K. Yang, J. Zhao, and J. P. Lu, Nano Lett. **4**, 561 (2004).
[13]H. Saeki, H. Tabata, and T. Kawai, Solid State Comm. **120**, 439 (2001).
[14]C. V. Ramana, S. Utsunomiya, R. C. Ewing, and U. Becker, Solid State Comm. **137**, 645 (2006).
[15]S. Surnev, M. G. Ramsey, and F. P. Netzer, Prog. Surf. Sci. **73**, 117 (2003).
[16]N. F. Mott, *Metal Insulator Transitions* (Taylor & Francis, London, 1974).
[17]D. B. McWhan, A. Menth, J. P. Remeika, W. F. Brinkman, and T. M. Rice, Phys. Rev. B **7**, 1920 (1973).
[18]D. B. McWhan, J. P. Remeika, T. M. Rice, W. F. Brinkman, J. P. Maita, and A. Menth, Phys. Rev. Lett. **27**, 941 (1971).
[19]P. D. Dernier, J. Phys. Chem. Solid. **31**, 2569 (1970).
[20]P. D. Dernier and M. Marezio, Phys. Rev. B **2**, 3771 (1970).
[21]D. M. Moffatt, J. P. Runt, A. Halliyal, and R. E. Newnham, J. Mater. Sci. **24**, 609 (1989).
[22]Y. Pan, G. Z. Wu, and X. S. Yi, J. Mater. Sci. **29**, 5757 (1994).
[23]C. Castellani, C. R. Natoli, and J. Ranninger, Phys. Rev. B **18**, 5001 (1978).
[24]C. Castellani, C. R. Natoli, and J. Ranninger, Phys. Rev. B **18**, 4967 (1978).
[25]C. Castellani, C. R. Natoli, and J. Ranninger, Phys. Rev. B **18**, 4945 (1978).
[26]J. Hubbard, Proc. R. Soc. Lond. A **276**, 238 (1963).
[27]J. Hubbard, Proc. R. Soc. Lond. A **281**, 401 (1964).
[28]M. S. Laad, L. Craco, and E. Muller-Hartmann, Phys. Rev. B **73**, 045109 (2006).
[29]S. Y. Ezhov, V. I. Anisimov, D. I. Khomskii, and G. A. Sawatzky, Phys. Rev. Lett. **83**, 4136 (1999).
[30]U. Schwingenschlogl, V. Eyert, and U. Eckern, Europhys. Lett. **64**, 682 (2003).
[31]I. S. Elfimov, T. Saha-Dasgupta, and M. A. Korotin, Phys. Rev. B **68**, 113105 (2003).
[32]J. H. Park, L. H. Tjeng, A. Tanaka, J. W. Allen, C. T. Chen, P. Metcalf, J. M. Honig, F. M. F. de Groot, and G. A. Sawatzky, Phys. Rev. B **61**, 11506 (2000).
[33]S. Di Matteo, N. B. Perkins, and C. R. Natoli, Phys. Rev. B **65**, 054413 (2002).
[34]Z. Ropka and R. J. Radwanski, Phys. B Condens. Matter **378–380**, 301 (2006).
[35]R. Shiina, F. Mila, F. C. Zhang, and T. M. Rice, Phys. Rev. B **63**, 144422 (2001).
[36]K. Held, I. A. Nekrasov, N. Blümer, V. I. Anisimov, and D. Vollhardt, Int. J. Mod. Phys. B **15**, 2611 (2001).
[37]K. Held, G. Keller, V. Eyert, D. Vollhardt, and V. I. Anisimov, Phys. Rev. Lett. **86**, 5345 (2001).
[38]V. I. Anisimov, D. E. Kondakov, A. V. Kozhevnikov, I. A. Nekrasov, Z. V. Pchelkina, J. W. Allen, S.-K. Mo, H.-D. Kim, P. Metcalf, S. Suga, A. Sekiyama, G. Keller, I. Leonov, X. Ren, and D. Vollhardt, Phys. Rev. B **71**, 125119 (2005).
[39]G. Keller, K. Held, V. Eyert, D. Vollhardt, and V. I. Anisimov, Phys. Rev. B **70**, 205116 (2004).
[40]D. Vollhardt, K. Held, G. Keller, R. Bulla, T. Pruschke, I. A. Nekrasov, and V. I. Anisimov, J. Phys. Soc. Jpn. **74**, 136 (2005).
[41]M. S. Laad, L. Craco, and E. Muller-Hartmann, Phys. Rev. Lett. **91**, 156402 (2003).
[42]G. Kresse, S. Surnev, J. Schoiswohl, and F. P. Netzer, Surf. Sci. **555**, 118 (2004).
[43]V. V. Ivanovskaya, A. N. Enyashin, and A. L. Ivanovskii, Mendeleev Comm. **13**, 5 (2003).
[44]V. V. Ivanovskaya, A. N. Enyashin, A. A. Sofronov, Y. N. Makurin, N. I. Medvedeva, and A. L. Ivanovskii, Solid State Comm. **126**, 489 (2003).
[45]A. C. Santulli, W. Xu, J. B. Parise, L. Wu, M. C. Aronson, F. Zhang, C.-Y. Nam, C. T. Black, A. L. Tiano, and S. S. Wong, Phys. Chem. Chem. Phys. **11**, 3718 (2009).
[46]P. Hohenberg and W. Kohn, Phys. Rev. B **136**, B864 (1964).
[47]W. Kohn and L. J. Sham, Phys. Rev. **140**, A1133 (1965).

[48]J. M. Soler, E. Artacho, J. D. Gale, A. Garcia, J. Junquera, P. Ordejon, and D. Sanchez-Portal, J. Phys. Condens. Matter **14**, 2745 (2002).
[49]N. Troullier and J. L. Martins, Phys. Rev. B **43**, 1993 (1991).
[50]W. R. Robinson, Acta Cryst. B **31**, 1153 (1975).
[51]L. F. Mattheiss, J. Phys. Condens. Matter **6**, 6477 (1994).
[52]M. Wierzbowska, D. Sánchez-Portal, and S. Sanvito, Phys. Rev. B **70**, 235209 (2004).
[53]V. Eyert, U. Schwingenschlögl, and U. Eckern, Europhys. Lett. **70**, 782 (2005).
[54]J. Schoiswohl, M. Sock, S. Surnev, M. G. Ramsey, F. P. Netzer, G. Kresse, and J. N. Andersen, Surf. Sci. **555**, 101 (2004).
[55]J. Schoiswohl, S. Surnev, F. P. Netzer, and G. Kresse, J. Phys. Condens. Matter **18**, R1 (2006).
[56]M. Schindler, F. C. Hawthorne, and W. H. Baur, Chem. Mater. **12**, 1248 (2000).
[57]F. J. Szalkowski and G. A. Somorjai, J. Chem. Phys. **56**, 6097 (1972).
[58]K. B. Lewis, S. T. Oyama, and G. A. Somorjai, Surf. Sci. **233**, 75 (1990).
[59]See Supplemental Material at http://link.aps.org/supplemental/10.1103/PhysRevB.86.125135 for a discussion about information and figures concerning theoretical methodology, constructs, electronic structure, surface terminations, and structural characterization of the nanowires we presented in this work.